

Reversionary Control Modes for the Mitigation of Failures in a Partially Turboelectric Aircraft Propulsion System

Donald L. Simon
Glenn Research Center, Cleveland, Ohio
Amy K. Chicatelli
HX5, LLC, Brook Park, Ohio
Santino J. Bianco
Glenn Research Center, Cleveland, Ohio
Marcus A. Horning
HX5, LLC, Brook Park, Ohio
Joseph R. Saus
Glenn Research Center, Cleveland, Ohio

NASA STI Program Report Series

Since its founding, NASA has been dedicated to the advancement of aeronautics and space science. The NASA scientific and technical information (STI) program plays a key part in helping NASA maintain this important role.

The NASA STI program operates under the auspices of the Agency Chief Information Officer. It collects, organizes, provides for archiving, and disseminates NASA's STI. The NASA STI program provides access to the NTRS Registered and its public interface, the NASA Technical Reports Server, thus providing one of the largest collections of aeronautical and space science STI in the world. Results are published in both non-NASA channels and by NASA in the NASA STI Report Series, which includes the following report types:

TECHNICAL PUBLICATION.

Reports of completed research or a major significant phase of research that present the results of NASA programs and include extensive data or theoretical analysis. Includes compilations of significant scientific and technical data and information deemed to be of continuing reference value. NASA counterpart of peer-reviewed formal professional papers but has less stringent limitations on manuscript length and extent of graphic presentations.

TECHNICAL MEMORANDUM.

Scientific and technical findings that are preliminary or of specialized interest, e.g., quick release reports, working papers, and bibliographies that contain minimal annotation. Does not contain extensive analysis.

CONTRACTOR REPORT. Scientific and technical findings by NASA-sponsored contractors and grantees.

CONFERENCE PUBLICATION. Collected papers from scientific and technical conferences, symposia, seminars, or other meetings sponsored or cosponsored by NASA.

SPECIAL PUBLICATION.

Scientific, technical, or historical information from NASA programs, projects, and missions, often concerned with subjects having substantial public interest.

TECHNICAL TRANSLATION.

English-language translations of foreign scientific and technical material pertinent to NASA's mission.

Specialized services also include organizing and publishing research results, distributing specialized research announcements and feeds, providing information desk and personal search support, and enabling data exchange services.

For more information about the NASA STI program, see the following:

 Access the NASA STI program home page at http://www.sti.nasa.gov



Reversionary Control Modes for the Mitigation of Failures in a Partially Turboelectric Aircraft Propulsion System

Donald L. Simon
Glenn Research Center, Cleveland, Ohio
Amy K. Chicatelli
HX5, LLC, Brook Park, Ohio
Santino J. Bianco
Glenn Research Center, Cleveland, Ohio
Marcus A. Horning
HX5, LLC, Brook Park, Ohio
Joseph R. Saus
Glenn Research Center, Cleveland, Ohio

Prepared for the Turbo Expo 2024 sponsored by American Society of Mechanical Engineers (ASME) London, United Kingdom, June 24–28, 2024

National Aeronautics and Space Administration

Glenn Research Center Cleveland, Ohio 44135

Acknowledgments

This work was conducted under the NASA Advanced Air	Vehicles Program,	Advanced Air	Transport '	Technology	Project, and
Aircraft Electrification Subproject.					

This work was sponsored by the Advanced Air Vehicles Program at the NASA Glenn Research Center.

Trade names and trademarks are used in this report for identification only. Their usage does not constitute an official endorsement, either expressed or implied, by the National Aeronautics and Space Administration.

Level of Review: This material has been technically reviewed by technical management.

This report is available in electronic form at https://www.sti.nasa.gov/ and https://ntrs.nasa.gov/

Reversionary Control Modes for the Mitigation of Failures in a Partially Turboelectric Aircraft Propulsion System

Donald L. Simon
National Aeronautics and Space Administration
Glenn Research Center
Cleveland, Ohio 44135

Amy K. Chicatelli HX5, LLC Brook Park, Ohio 44142

Santino J. Bianco
National Aeronautics and Space Administration
Glenn Research Center
Cleveland, Ohio 44135

Marcus A. Horning HX5, LLC Brook Park, Ohio 44142

Joseph R. Saus National Aeronautics and Space Administration Glenn Research Center Cleveland, Ohio 44135

Abstract

In support of emission and fuel burn reduction goals, the aviation industry is actively pursuing the advancement of electrified aircraft propulsion (EAP) technology. This includes turboelectric and hybrid electric propulsion designs that combine gas turbine engine and electrical system hardware. Such architectures exhibit a high degree of coupling between subsystems. This drives the need for system-level control strategies to ensure the safe, coordinated, and efficient operation of all subsystems. The design and certification of any aircraft propulsion system requires that all potential subsystem failures are identified, and the hazards posed by these failures are appropriately mitigated. This requirement is particularly challenging for EAP systems due to their integrated nature. One approach to assist in EAP failure mitigation is the inclusion of automated reconfiguration capabilities within the propulsion control system. Such control modes, referred to as reversionary control modes, are designed to automatically detect failures and activate backup control modes upon failure detection. This paper covers the design and evaluation of reversionary control mode logic developed for a partially turboelectric propulsion concept. Test results from a real-time hardware-in-the-loop evaluation of the concept are also presented and discussed. The

results show that the developed reversionary control logic can successfully detect and mitigate subsystem failures in a representative environment that includes actual electrical system hardware.

Nomenclature

Acronyms

ASMICS	Adaptive sliding mode impedance controller
	with scaling
DC	Direct current
EAP	Electrified aircraft propulsion
HIL	Hardware-in-the-loop
HP	High-pressure
HPC	High-pressure compressor
HPX	Horsepower extraction
HyPER	Hybrid Propulsion Emulation Rig
LP	Low-pressure
LPC	Low-pressure compressor
NPSS	Numerical propulsion system simulation
PI	Proportional plus integral
PLA	Power lever angle
SLS	Sea level static

STARC-ABL Single-aisle turboelectric aircraft with aft

boundary layer propulsion

T-MATS Toolbox for the modeling and analysis of

thermodynamic systems

VAFN Variable area fan nozzle VBV Variable bleed valve

Parameters

A, B, C	State-space matrices
N_{1c}	Corrected turbofan fan speed
\dot{N}_{1c}	Corrected turbofan fan speed derivative
N_{2c}	Corrected turbofan low-pressure shaft speed
\dot{N}_{2c}	Corrected turbofan low-pressure shaft speed derivative
N_{3c}	Corrected turbofan core speed
\dot{N}_{3c}	Corrected turbofan core speed derivative
N_{tc}	Corrected tailfan speed
\dot{N}_{tc}	Corrected tailfan speed derivative
Ps3	Turbofan HPC exit static pressure
Q_m	Tailfan motor torque
T4	Turbine inlet temperature
u,x,y	State-space input, state, and output vectors
W_f	Fuel flow rate
γ	Ratio of tailfan to turbofan speed variation
Δ	Deviation about trim condition

1.0 Introduction

Electrified aircraft propulsion (EAP) relies on the use of electrical power to produce aircraft thrust. It holds great potential for the reduction of aircraft fuel burn, emissions, and noise. Currently, NASA and other organizations are actively working to advance technologies necessary to bring EAP designs to reality (Refs. 1 and 2). This includes turboelectric and hybrid electric designs that combine gas turbine engines and electrical components. A requirement for the development of any civil aircraft is that all potential hazards in the design are identified and appropriately mitigated to ensure that the system is safe (Refs. 3 and 4). EAP designs will introduce new flight critical propulsion components and architectures, often with a high degree of coupling between subsystems. This raises the concern of cascading failure scenarios where one subsystem failure causes subsequent failures throughout the architecture. Such scenarios must be identified and shown to be appropriately mitigated as part of the aircraft safety assessment and design process (Refs. 5 and 6).

To facilitate failure mitigation, redundancy within an EAP architecture will be required to assure that the propulsion

system can continue to deliver adequate thrust in the event of a failure. Passive hardware fault management techniques such as circuit breakers, current limiters, and power electronics technology will also be critical (Refs. 7 and 8). Additionally, the propulsion control system is expected to play a significant role in assuring that EAP systems comply with the airworthiness standards set forth by regulatory agencies. This includes logic to automatically detect system failures and revert to alternate backup control modes to enable safe failure mitigation. Such backup control modes are common in modern aircraft engine electronic control systems and are often referred to as "reversionary" control modes (e.g., see Refs. 9 to 11). Compared to conventional aircraft engines, EAP systems are expected to present unique reversionary control development needs due to their complex integrated nature.

Past NASA efforts focused on the development of EAP system reversionary control strategies have considered both parallel hybrid and partially turboelectric designs. Reference 12 focused on a parallel hybrid architecture consisting of a twospool turbofan engine with electric machines attached to the high-pressure (HP) and low-pressure (LP) shafts, a high voltage direct current (DC) power bus, and an energy storage device. This study demonstrated that reversionary control strategies could prevent engine overtemperature events and reduce the risk of compressor stalls. References 6 and 13 presented reversionary control strategies for the NASA Single-aisle Turboelectric AiRCraft with Aft Boundary Layer propulsor (STARC-ABL) concept aircraft. The STARC-ABL is a partially turboelectric design consisting of two wing mounted geared turbofan engines and an electric motor driven boundary layer ingesting tailfan propulsor (Refs. 14 and 15). It exhibits coupling between subsystems and past analysis has shown that unmitigated subsystem failures in this concept can cascade into catastrophic events (Ref. 6). The STARC-ABL reversionary control study in Reference 6 was preliminary in nature and only considered failure mitigation at a single flight condition. Reference 13 considered a modified STARC-ABL concept that included energy storage and applied the NASA-developed Turbine Electrified Energy Management control concept (Ref. 16). Neither Reference 6 nor Reference 13 considered failure detection and mitigation during transient operation. Follow-on NASA work has added several enhancements to the STARC-ABL reversionary control logic. This includes the addition of failure detection logic and an integrated control design approach that in combination provide robust full-flight envelope detection and mitigation of potential STARC-ABL subsystem failures. Initial results from a flight simulator evaluation of the STARC-ABL reversionary control logic were presented in Reference 17. This paper provides details regarding the logic's overall design and operation.

The remaining sections of this paper are organized as follows. An overview of the STARC-ABL concept is provided in Section 2.0 and a description of its baseline propulsion control design is given in Section 3.0. This is followed by a description of STARC-ABL failure modes and effects in Section 4.0. Section 5.0 discusses reversionary control logic including failure detection logic and the reversionary control modes. Section 6.0 presents results from a real-time hardware-in-theloop (HIL) test conducted to evaluate the effectiveness of the reversionary control fault mitigation strategy at select operating points. This test included a subscale representation of the STARC-ABL's electrical system and simulated turbomachinery elements. Finally, a discussion is provided in Section 7.0 followed by conclusions in Section 8.0.

2.0 STARC-ABL Overview

An image of the STARC-ABL aircraft and a block diagram of its propulsion system are provided in Figure 1 and Figure 2, respectively. The two turbofan engines in this single-aisle commercial airliner concept serve the dual purpose of producing thrust and supplying mechanical offtake power delivered to electric generators attached to their LP shafts. Electrical power produced by the generators is transported over a 1000 V DC bus to a motor controller and inverter. The motor controller operates a 3500 hp motor that drives the tailfan. The



Figure 1.—STARC-ABL Aircraft.

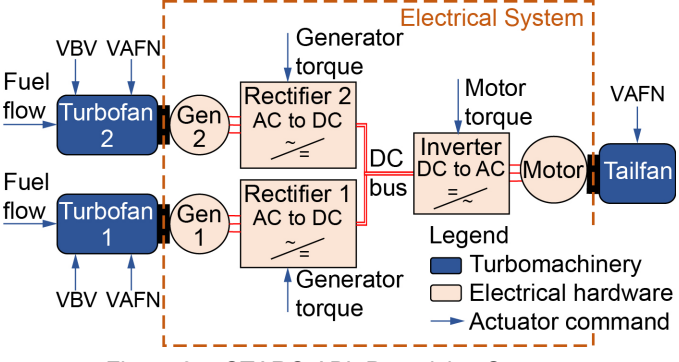


Figure 2.—STARC-ABL Propulsion System.

end-to-end efficiency of the STARC-ABL's electrical system is approximately 90 percent. System inputs include fuel flow supplied to each turbofan and torque commands provided to each generator controller and the tailfan motor controller. Additionally, each turbofan is equipped with a variable bleed valve (VBV) installed between its low-pressure compressor (LPC) and high-pressure compressor (HPC) and a variable area fan nozzle (VAFN) installed in its bypass stream. The tailfan is also equipped with a VAFN actuator, which is installed aft of its fan module.

3.0 Baseline STARC-ABL Control Design

Original NASA publications on the STARC-ABL concept (Refs. 14 and 15) are system studies focused on steady-state performance benefits. They are based on a nonlinear steadystate model of the STARC-ABL coded in the Numerical Propulsion System Simulation (NPSS) environment (Ref. 18) and do not explicitly discuss transient operation or a control concept of operations for the propulsion system. To address this need, a system-level integrated control design for the STARC-ABL propulsion system has been developed as detailed in Reference 19. This design has been shown to promote coordinated operation of the tailfan and turbofan subsystems during both steady-state and transient operation under nominal (failure free) conditions. It will serve as the "baseline" architecture that the reversionary control developed in this study will be compared against. An overview of the transient propulsion system model used for developing and evaluating the baseline control is given in Section 3.1, followed by a discussion of the design's variable geometry and thrust schedules in Section 3.2, and its closed-loop control strategy in Section 3.3.

3.1 Nonlinear Transient Propulsion System Model

The baseline control presented in Reference 19 was designed and evaluated using a nonlinear transient model of the STARC-ABL propulsion system derived from the steady-state NPSS model used in Reference 15. The transient model is implemented in MATLAB® Simulink® (MathWorks, Natick, MA) using the NASA-developed Toolbox for the Modeling and Analysis of Thermodynamic Systems (T-MATS) (Ref. 20) and a power flow modeling approach (Ref. 21). T-MATS is used to model the turbomachinery components, while the power flow approach is used to model electrical system components at turbomachinery time-scales. Shaft dynamics are also included to enable simulation of transient operation.

3.2 Variable Geometry and Thrust Schedules

The baseline controller applies schedules for the VBV and VAFN variable geometry actuators consistent with those of the original NPSS model. The turbofan VBV is open-loop scheduled based on turbofan corrected fan speed, N_{1c} , and is designed to maintain a minimum turbofan LPC stall margin of 10 percent. The turbofan VAFN is also open-loop scheduled based on N_{1c} while the tailfan VAFN is open-loop scheduled based on corrected tailfan speed, N_{tc} . The applied VAFN schedules ensure that the fan modules of the respective subsystems follow an operating line of near optimal efficiency.

Power lever angle (PLA) thrust schedules for the STARC-ABL's turbofan and tailfan subsystem controllers are also derived from the original NPSS model. These schedules apply corrected fan speeds (N_{1c} for the turbofans and N_{tc} for the tailfan) as the thrust feedback parameters scheduled as a function of PLA throttle input. The defined PLA thrust schedules promote coordinated steady-state operation of the turbofan and tailfan subsystems throughout the STARC-ABL's flight envelope (0 to 43 k ft altitude and 0 to 0.82 Mach), while maintaining tailfan motor power below its maximum 3500 hp limit.

3.3 Integrated Closed-Loop Control Design

The control concept of operations applied in Reference 19 assumes that the tailfan motor consumes the necessary power from the DC bus to reach its commanded operating state, while the turbofan generators act to hold a target 1000 V DC bus voltage. With this assumption, the electrical power system exhibits an aft-to-forward coupling with any changes in the tailfan power demand resulting in a corresponding change in the amount of power the generators extract from the turbofan LP shafts. The amount of power extraction the turbofans can support is dependent on their operating state. Extracting too much power can cause HPC stalls while extracting too little power can cause LPC stalls. This requires coordinated control of the turbofan and tailfan subsystems, especially during transient operation. To address this concern, Reference 19 applied a single throttle input control strategy where both turbofans receive identical throttle inputs while the tailfan receives a synthesized throttle input calculated as a function of the average fan speed of the two turbofans. This approach maintains coordinated operation between the turbofans and the tailfan during transients while allowing the turbofan fuel control design to be simplified to a single-input single-output linear problem.

The control design process includes the development of proportional plus integral (PI) fan speed setpoint controllers for the tailfan and turbofan. Individual linear setpoint controllers are designed at multiple points spanning the STARC-ABL's operating envelope. To support this control design process, linear state-space models of the following form are extracted from the nonlinear T-MATS model at each design point:

$$\dot{x} = A \cdot \underbrace{(x - x_{trim})}_{\Delta x} + B \cdot \underbrace{(u - u_{trim})}_{\Delta u} \\
\underbrace{(y - y_{trim})}_{\Delta y} = C \cdot \underbrace{(x - x_{trim})}_{\Delta x} \tag{1}$$

with state variable vector, x, control input vector, u, and sensed measurement vector, y. Trim conditions in those same vectors are denoted as x_{trim} , u_{trim} , and y_{trim} , and deviations (Δ 's) about those trim conditions are denoted as Δx , Δu , and Δy . Throughout the remainder of this paper the Δ terms are dropped for simplification. Expanding the state-space model vectors and matrices to show individual elements yields Equation (2). Here, the dynamics of only a single turbofan plus the tailfan are considered. This simplification is possible due to the symmetric operating nature of the two turbofans.

$$\underbrace{\begin{bmatrix} \dot{N}_{2c} \\ \dot{N}_{3c} \\ \dot{N}_{tc} \end{bmatrix}}_{\dot{x}} = \underbrace{\begin{bmatrix} A_{11} & A_{12} & 0 \\ A_{21} & A_{22} & 0 \\ 0 & 0 & A_{33} \end{bmatrix}}_{A} \underbrace{\begin{bmatrix} N_{2c} \\ N_{3c} \\ N_{tc} \end{bmatrix}}_{x} + \underbrace{\begin{bmatrix} B_{11} & B_{12} \\ B_{21} & 0 \\ 0 & B_{32} \end{bmatrix}}_{B} \underbrace{\begin{bmatrix} W_f \\ Q_m \end{bmatrix}}_{u}$$

$$\underbrace{\begin{bmatrix} N_{1c} \\ N_{tc} \end{bmatrix}}_{y} = \underbrace{\begin{bmatrix} C_{11} & 0 & 0 \\ 0 & 0 & 1 \end{bmatrix}}_{c} \underbrace{\begin{bmatrix} N_{2c} \\ N_{3c} \\ N_{tc} \end{bmatrix}}_{x}$$
(2)

The state vector, x, includes turbofan corrected LP shaft speed, N_{2c} , turbofan corrected core speed, N_{3c} , and tailfan corrected speed, N_{tc} . The input vector, u, includes turbofan fuel flow rate, W_f , and tailfan motor torque, Q_m . The output vector, y, includes N_{1c} and N_{tc} . It is noted that within the STARC-ABL's geared turbofan design, N_{2c} and N_{1c} are directly proportional and related by a gear ratio expressed as $N_{2c} = 2.7 \cdot N_{1c}$. The aft-to-forward coupling in the system is reflected in the B_{12} term of the B matrix in Equation (2). This shows that any change in motor torque Q_m will affect the turbofan's N_{2c} state.

A STARC-ABL closed-loop control architecture can be drawn in block diagram form as illustrated in Figure 3. Here, the turbofan detail is expanded to show integrator blocks and state-space matrix elements from Equation (2). Transfer functions reflecting dynamics of the fuel actuator and the tailfan are denoted as F(s) and $G_t(s)$, respectively. Sensor dynamics as well as motor and generator actuator dynamics are excluded from the figure and the control design process as they are assumed to occur on a time scale considerably faster than the turbofan and tailfan shaft dynamics. Also excluded are VBV and VAFN dynamics as they are assumed to operate on-schedule. The setpoint control design process requires design of

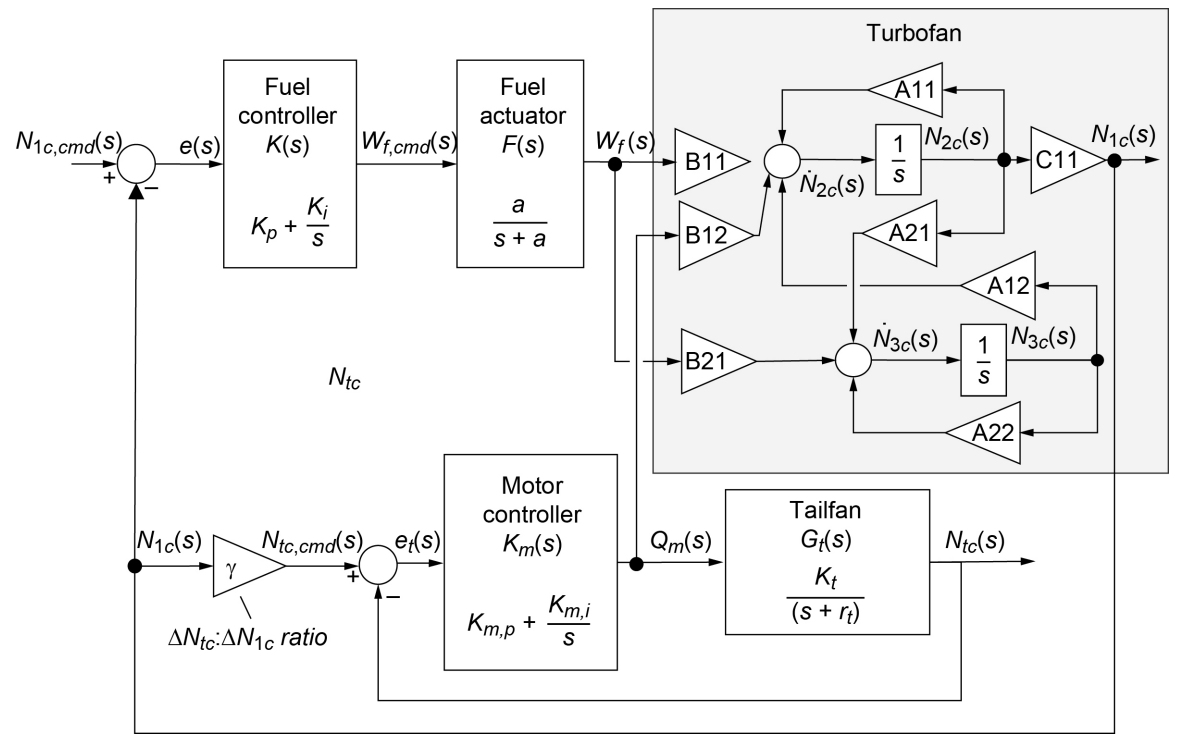


Figure 3.—STARC-ABL Closed-Loop Control Architecture.

the two PI controllers, denoted as K(s) for the turbofan fuel controller and $K_m(s)$ for the tailfan motor controller. The gain block, γ , reflects the fractional change in commanded tailfan corrected speed, $N_{tc,cmd}$, based on a change in turbofan corrected fan speed, N_{1c} , which is consistent with the choice of constructing a synthesized tailfan PLA based on the average N_{1c} of the two turbofans. This N_{tc} : N_{1c} ratio can be thought of as the small perturbation relationship between turbofan and tailfan speeds at a given design point. Consistent with Equation (2), Motor torque, $Q_m(s)$, is shown as an input feeding directly into both the tailfan and the turbofan.

From Figure 3, a loop transfer function, T(s), relating $N_{tc,cmd}$ to $Q_m(s)$ can be produced as shown in Equation (3). As detailed

$$T(s) = \frac{Q_m(s)}{N_{tc.cmd}(s)} = \frac{K_m(s)}{I + K_m(s)G_t(s)}$$
(3)

in Reference 19, T(s) can be combined with other elements of Figure 3 to produce the following single-input single-output transfer function relating turbofan fuel flow rate input, W_f , to turbofan N_{1c} output:

$$\frac{N_{1c}(s)}{W_f(s)} = \frac{B_{11}C_{11}\left(s + \frac{A_{12}B_{21}}{B_{11}} - A_{22}\right)}{(s - A_{11})(s - A_{22}) - A_{12}A_{21} - C_{11}\gamma T(s)B_{12}(s - A_{22})} \tag{4}$$

Tailfan power extraction coupling effects are captured in the $C_{11}\gamma T(s)B_{12}(s-A_{22})$ portion of the Equation (4) denominator.

In addition to the setpoint controller, the baseline STARC-ABL fuel control system also includes acceleration and deceleration schedules based on a fan speed derivative, \dot{N}_{1c} , plus a minimum HPC exit static pressure (Ps3) limiter. The tailfan motor controller includes its setpoint controller plus a maximum horsepower limiter. Setpoint, transient, and limit controllers are designed at multiple operating points spanning the STARC-ABL operating envelope. They are then combined in a piecewise linear gain scheduling fashion to provide nonlinear full operating envelope control functionality (Ref. 22). Throughout a flight, the control system automatically switches its operating mode between setpoint, transient, and limit controllers by applying conventional maximum-minimum mode selection logic to determine which control regulator is active at any instant in time (Refs. 22 and 23). Smooth transition between the controllers is managed by integrator windup protection-based bumpless transfer logic.

4.0 Subsystem Failure Modes and Effects

A high-level assessment of the STARC-ABL's subsystem failure modes and their effects was conducted in Reference 6 and is summarized in Table I. Here, only abrupt complete functional failures of a single subsystem are considered as

]	TABLE I.—STARC-ABL FAILURE MODES AND EFFECTS						
		Failed subsystem					
		Turbofan 1 Failed	Turbofan 2 Failed	Power string 1 failed	Power string 2 failed	Tailfan failed	
stems	Turbofan 1	Failed	Increased HPX	No HPX	Increased HPX	No HPX	
r subsystems	Turbofan 2	Increased HPX	Failed	Increased HPX	No HPX	No HPX	
Coupled failure effects on other	Power string 1	No electric power	Increased electric power	Failed	Increased electric power	No electric power	
	Power string 2	Increased electric power	No electric power	Increased Electric Power	Failed	No electric power	
Coupled	Tailfan	Reduced electric power	Reduced electric power	Reduced electric power	Reduced electric power	Failed	

opposed to failures resulting in a partial loss of functionality or failures occurring simultaneously in multiple subsystems. The failures are listed in the Table I columns and include a failure of turbofan 1, turbofan 2, power string 1, power string 2, or the tailfan. The rows reflect the coupled effects of each failure on other subsystems when the system is operating under the original baseline control design.

The baseline STARC-ABL configuration and control concept can lead to either increased or no turbofan horsepower extraction (HPX) upon subsystem failures. Of particular concern is the failure of either a turbofan or a power string. Under such failures, the tailfan speed controller would attempt to draw 100 percent of the necessary power to hold the commanded tailfan speed setpoint from the remaining nominally operating turbofan and its power string. This could happen very rapidly, leading to a compressor stall and shutdown of the remaining healthy engine—a potentially catastrophic event. Avoidance of this scenario would require an extremely fast responding fault detection and accommodation strategy, which may not be possible at the time-scales of gas turbine engine controls. To alleviate this concern, this study partitions the STARC-ABL DC power bus and the tailfan motor into two separate parallel power strings. Each string is supplied power by an individual turbofan generator and contributes 50 percent of the total electrical power delivered to the tailfan. This revised configuration is shown in Figure 4. In contrast to Figure 2 which contained a single inverter driving the tailfan motor, Figure 4 shows the motor equipped with two redundant

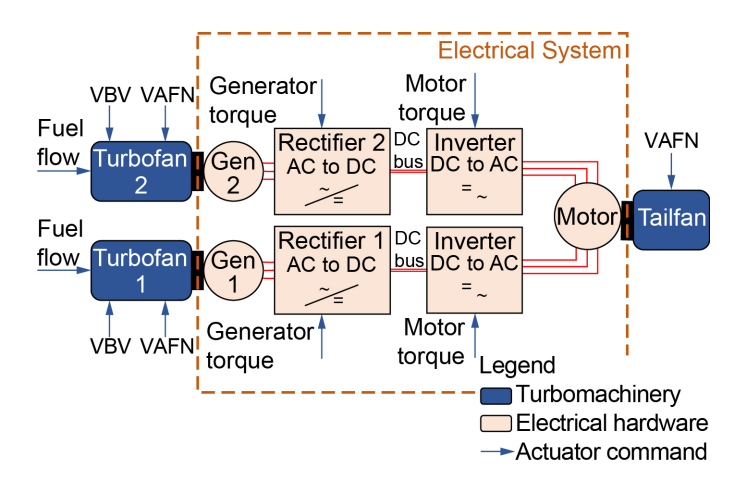


Figure 4.—Revised STARC-ABL Propulsion System.

field windings each energized by a separate power string. In the event of a single turbofan or power string failure, the remaining healthy turbofan and power string can still provide electrical power to the tailfan. This allows the tailfan to continue to operate in the presence of such failures, albeit at a reduced maximum thrust level compared to the nominal design. In addition to the added power string redundancy, it was assumed that each turbofan generator and power string could be operated at 125 percent of its maximum continuous power level for up to 5 min. This 5-min maximum power operational time is consistent with typical turbofan maximum thrust operating limits (Ref. 24) and offers slightly increased thrust output under contingency operating scenarios.

5.0 Detection Logic and Reversionary Control Modes for Failure Mitigation

Given the revised STARC-ABL propulsion architecture of Figure 4, steps were taken to develop associated failure detection and reversionary control logic to mitigate potential failure events. This assumed that each turbofan control system is designed to operate either nominally (Mode 0) or in a reversionary control mode including no HPX (Mode 1) or increased HPX (Mode 2). Similarly, the tailfan control system could operate either nominally (Mode 0) or a reversionary control mode of reduced available power (Mode 1). The specific control modes that are activated upon the detection of any individual subsystem failure are shown in Table II. Here, the columns denote the identified failed subsystem, and the rows denote the corresponding control mode activated for the turbofan and tailfan subsystems.

TABLE II.—NOMINAL AND REVERSIONARY CONTROL MODES FOR STARC-ABL SUBSYSTEMS

	MODES FOR STARC-ABE SOBSTSTEMS						
	Nominal		Failed subsystem				
	Nominal	Turbofan 1 failed	Turbofan 2 failed	Power system 1 failed	Power system 2 failed	Tailfan Failed	
Turbofan 1	Mode 0	N/A	Mode 2	Mode 1	Mode 2	Mode 1	
Turbofan 2	Mode 0	Mode 2	N/A	Mode 2	Mode 1	Mode 1	
Tailfan	Mode 0	Mode 1	Mode 1	Mode 1	Mode 1	N/A	

5.1 Failure Detection and Control Mode Activation Logic

The reversionary control system provides accurate and timely diagnosis of subsystem failures and system-level coordination of the control modes activated within the subsystems. In this study, the logic applied to activate the appropriate control mode for an individual turbofan's control system is shown in Equation (5). By default, the system begins in Mode 0 operating under nominal baseline control. The control system is updated on a 15 ms control cycle interval. During each control cycle, detection logic assesses the sensed HPX load that the generator applies to the LP shaft of the turbofan. If the HPX load drops below 100 hp and persists below that threshold for three control cycle counts (45 ms), the turbofan's control system will automatically switch to Mode 1—the reversionary control mode associated with no generator HPX taken from the turbofan's LP shaft (see Table II). This logic will cause the turbofan controller to transition to Mode 1 if either its attached power string or the tailfan experiences a failure. The three control cycle count persistency is added to help avoid nuisance false alarms caused due to measurement noise. Upon transition to Mode 1, the generator in the power string attached to the turbofan is disabled from further use. In addition to monitoring generator HPX load, the logic also monitors the control mode of the companion turbofan installed on the opposite wing. If a turbofan's control system is operating in Mode 0 and the companion turbofan's control system is persistently operating in Mode 1 for 10 control cycle counts (150 ms) the turbofan's control system will switch to Mode 2-the control mode associated with extra generator HPX. This switch to Mode 2 will permit HPX loads up to 125 percent of nominal while adhering to a maximum turbine inlet temperature limit. The 10 cycle persistency requirement for an engine's control system to transition to Mode 2 is intentionally longer than the three cycle persistency requirement to transition to Mode 1 to allow for the possibility of a tailfan failure. Upon a tailfan failure, both engine controllers should ultimately transition to Mode 1 (see Table II). However, this transition may not occur at the same time due to signal measurement noise. The 10 cycle persistency guards against an engine controller erroneously transitioning from Mode 0 to Mode 2 upon a tailfan failure.

Reversionary control mode activation logic for the tailfan controller is shown in Equation (6). The tailfan controller also begins in a nominal control Mode 0. Activation logic monitors the current active control mode of both turbofans. If either turbofan control system switches out of its nominal control Mode 0 into Mode 1, the tailfan controller immediately transitions to its control Mode 1—operation under reduced maximum available power. If the companion Turbofan control system later transitions to Mode 2, the tailfan controller will remain in Mode 1 but the maximum power limit of the power string attached to the turbofan operating in Mode 2 will increase to 125 percent.

The reversionary control logic assumes that if a subsystem failure is detected, the power string components associated with that failed subsystem will be disabled and remain inoperable unless the failed subsystem undergoes a successful in-flight restart. Given this assumption, all control mode transitions under failure conditions are unidirectional. The turbofan controller can transition directly from its Mode 0 to either Mode 1 or Mode 2. Transitions from Mode 2 to Mode 1 are also permissible. However, once operating in Mode 1, which results in the attached power string being disabled, the system cannot transition back to Mode 0 or Mode 2. Similarly, if the tailfan controller transitions to Mode 1, it cannot transition back to Mode 0. The current implementation of the reversionary control design does not yet include logic to facilitate a transition from a reversionary control mode back to nominal. Follow-on work to add this functionality is recommended.

5.2 Reversionary Control Mode Design

Figure 5 shows STARC-ABL linear state-space models and trim conditions to illustrate the variation in system dynamics under different subsystem failure scenarios and control modes. For this example, all linear state-space models are extracted

$$x_{trim} = \begin{bmatrix} N_{2c} \\ N_{3c} \\ N_{tc} \end{bmatrix} = \begin{bmatrix} 11340 \\ 22430 \\ 2178 \end{bmatrix} \quad A = \begin{bmatrix} -2.478 & 2.001 & 0 \\ 2.901 & -15.516 & 0 \\ 0 & 0 & 3.103 \end{bmatrix}$$

$$u_{trim} = \begin{bmatrix} W_f \\ Q_m \end{bmatrix} = \begin{bmatrix} 4388 \\ 8440 \end{bmatrix} \quad B = \begin{bmatrix} 1.466 & -0.165 \\ 6.282 & 0 \\ 0 & 0.398 \end{bmatrix}$$

$$y_{trim} = \begin{bmatrix} N_{1c} \\ N_{tc} \end{bmatrix} = \begin{bmatrix} 4200 \\ 2178 \end{bmatrix} \quad C = \begin{bmatrix} 0.370 & 0 \\ 0 & 1 \end{bmatrix}$$
(a)

$$x_{trim} = \begin{bmatrix} N_{2c} \\ N_{3c} \\ N_{tc} \end{bmatrix} = \begin{bmatrix} 11340 \\ 22214 \\ - \end{bmatrix} \qquad A = \begin{bmatrix} -3.207 & 3.333 & - \\ 5.053 & -20.532 & - \\ - & - & - \end{bmatrix}$$

$$u_{trim} = \begin{bmatrix} W_f \\ Q_m \end{bmatrix} = \begin{bmatrix} 3789 \\ - \end{bmatrix} \qquad B = \begin{bmatrix} 1.498 & - \\ 6.737 & - \\ - & - \end{bmatrix}$$

$$y_{trim} = \begin{bmatrix} N_{1c} \\ N_{tc} \end{bmatrix} = \begin{bmatrix} 4200 \\ - \end{bmatrix} \qquad C = \begin{bmatrix} 0.370 & 0 \\ 0 & 1 \end{bmatrix}$$
(b)

$$x_{trim} = \begin{bmatrix} N_{2c} \\ N_{3c} \\ N_{tc} \end{bmatrix} = \begin{bmatrix} 11340 \\ 22520 \\ 1866 \end{bmatrix} \quad A = \begin{bmatrix} -2.082 & 1.075 & 0 \\ 0.7119 & -10.547 & 0 \\ 0 & 0 & -2.551 \end{bmatrix}$$

$$u_{trim} = \begin{bmatrix} W_f \\ Q_m \end{bmatrix} = \begin{bmatrix} 4551 \\ 6165 \end{bmatrix} \qquad B = \begin{bmatrix} 1.470 & -0.282 \\ 6.179 & 0 \\ 0 & 0.398 \end{bmatrix}$$

$$y_{trim} = \begin{bmatrix} N_{1c} \\ N_{tc} \end{bmatrix} = \begin{bmatrix} 4200 \\ 1866 \end{bmatrix} \qquad C = \begin{bmatrix} 0.370 & 0 \\ 0 & 1 \end{bmatrix}$$
(c)

Figure 5.—Comparison of state-space models for nominal and reversionary control modes (sea level static, 4200 rpm N_{1c} operating point). (a) Nominal (turbofan mode 0 and tailfan mode 0). (b) Attached power string or tailfan failure (turbofan mode 1). (c) Opposite Turbofan or opposite power string failure (turbofan mode 2 and tailfan mode 1).

from the nonlinear T-MATS STARC-ABL model at the sea level static (SLS) and $N_{1c} = 4200$ rpm operating point. The resulting linear models take the form of the state-space model previously introduced in Equations (1) and (2). Figure 5(a) shows the state-space model when the system is operating failure free with all subsystem controllers in their nominal control Mode 0. Figure 5(b) shows the state-space model for an individual turbofan operating in control Mode 1 with a failure either in its attached power string or the tailfan. Tailfan loading and dynamics are omitted from Figure 5(b). Figure 5(c) shows the state-space model for an individual turbofan operating in its control Mode 2 and the tailfan in its control Mode 1 with a failure in the opposite engine or power string. Comparing the trim vectors and state-space matrix elements illustrates the variation in steady-state operation and system dynamics that is

occurring across these three scenarios. To facilitate control design, linear state-space models spanning the STARC-ABL's operating envelope are produced for each of the scenarios. These models are then used to design a complete control system for the STARC-ABL, including the nominal baseline control and the reversionary control modes.

As shown in Table II, any turbofan or power string failure will result in the tailfan operating in its reversionary control Mode 1. In this control mode, all tailfan motor power is supplied by a single turbofan and its attached power string. This requires a revised tailfan PLA to N_{tc} thrust schedule that is compatible with the power production capabilities of a single turbofan and its power string. A comparison of the nominal (Mode 0) and reversionary (Mode 1) PLA to N_{tc} schedules for the tailfan at SLS conditions is provided in Figure 6 along with resultant effects on other system parameters. The PLA to N_{tc} schedule comparison, which is provided in Figure 6(a), shows the tailfan operating at a lower speed in control Mode 1. The total tailfan motor power contributed by the combination of power string 1 and power string 2 (see Figure 4) is shown in Figure 6(b). Under Mode 0 operation, up to 3500 hp of total motor power can be delivered to the tailfan with each string contributing 50 percent (1750 hp). Under Mode 1 operation, the maximum total motor power is reduced to 2188 hp with all power provided by a single power string attached to one of the motor's two field windings. Turbofan generator LP shaft HPX and the ratio of generator LP shaft HPX to low pressure turbine hp input (denoted HPX ratio) are shown in Figure 6(c) and (d), respectively, for turbofans operating in control Modes 0, 1, or 2. Under nominal conditions (Mode 0) a maximum generator LP shaft HPX level of 1942 hp is reached when total tailfan motor power is at its 3500 hp operating limit. Under failure conditions, the LP shaft HPX of the turbofan operating in control Mode 2 increases to 2428 hp while the companion engine's LP shaft HPX drops to 0 hp and its controller operates in Mode 1. Figure 6(d) shows an elevated LP shaft HPX ratio for Mode 2 compared to Mode 0 at the higher PLA settings when the motor power limit is encountered. Once PLA is reduced to the point where the turbofan LP HPX ratio of 28 percent is encountered, that ratio is maintained through idle.

Turbofan VBV actuator position is open-loop scheduled as a function of N_{1c} to maintain a minimum steady-state LPC stall margin of 10 percent. As LPC stall margin is dependent on the amount of generator HPX demand placed on a turbofan's LP shaft, modified turbofan VBV schedules are necessary for the reversionary control modes. VBV schedules and LPC stall margins for all control modes are shown in Figure 7 for the SLS condition. The VBV is fully closed and LPC stall margin is greater than 10 percent at high N_{1c} speeds in all modes. The VBV remains closed as N_{1c} is reduced until LPC stall margin reaches 10 percent. At this point, the VBV schedule transitions

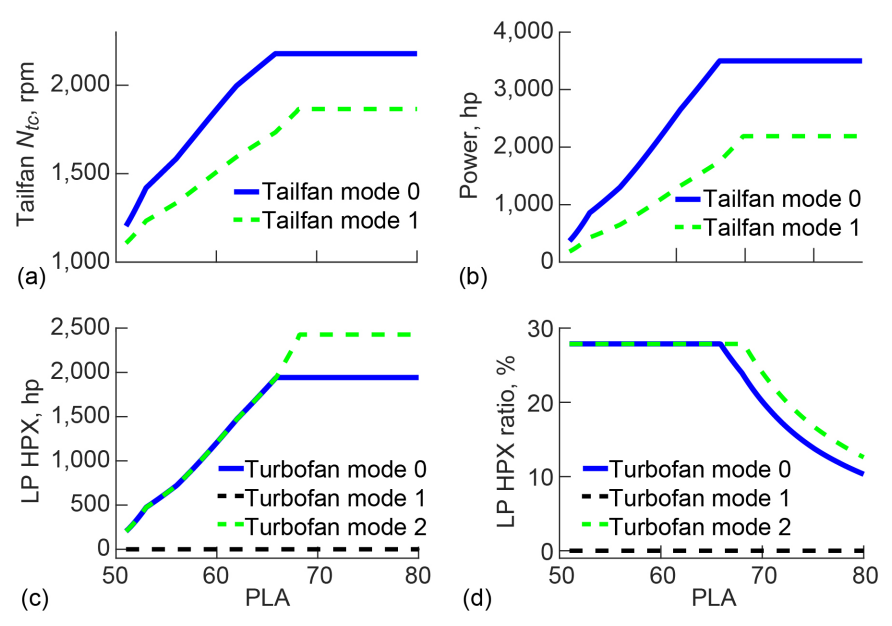


Figure 6.—Comparison of nominal and reversionary control thrust schedule effects (SLS condition). (a) Tailfan *Ntc.* (b) Total tailfan motor power. (c) Turbofan LP HPX. (d) Turbofan LP HPX ratio.

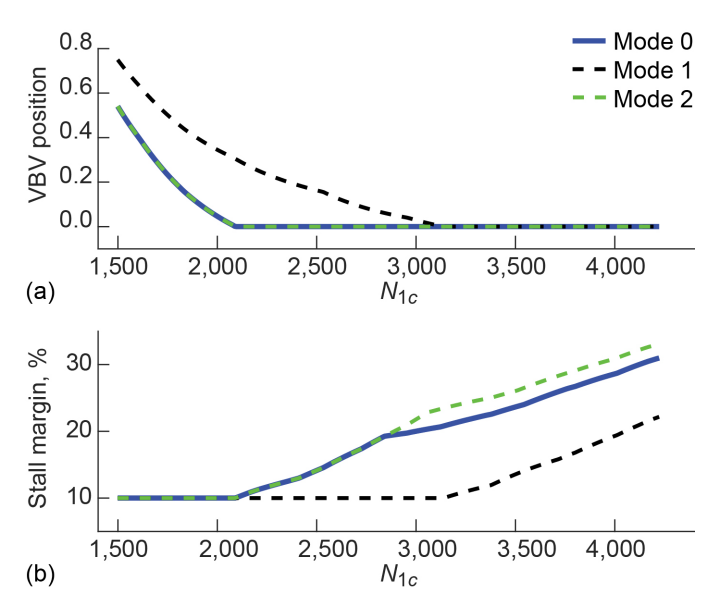


Figure 7.—Nominal and reversionary control VBV scheduling and LPC stall margin (SLS condition). (a) Turbofan VBV schedule. (b) Turbofan LPC stall margin.

from closed to opening to maintain a 10 percent LPC stall margin. For reversionary control Mode 1 (the failure case with no LP shaft HPX), the point where the VBV transitions from closed to opening occurs at a higher N_{1c} speed. The VBV schedules for Mode 0 and Mode 2 are identical at this condition as both control modes are operating on the 28 percent LP shaft HPX ratio schedule at the N_{1c} speed when the 10 percent LPC stall margin is encountered.

All turbofan control modes apply identical \dot{N}_{1c} acceleration and deceleration schedules. This allows similar N_{1c} transient response between the two turbofans to be maintained under nominal operation or during failure scenarios with one turbofan in control Mode 1 and the opposite turbofan in control Mode 2.

The design process for each control mode was performed over a range of operating conditions and combined with the failure detection and control mode transition logic to provide full flight envelope functionality. To promote stability, the PI control loops within all control modes were designed to provide a minimum of 8 dB gain margin and 55 degrees phase margin. This, in combination with the included integrator windup protection logic, was found to promote smooth transition between the controllers.

6.0 Real-Time Hardware in the Loop Test

To evaluate the performance of the newly developed STARC-ABL reversionary control logic, a HIL test was performed at the Hybrid Propulsion Emulation Rig (HyPER) located at the NASA Glenn Research Center in Cleveland, Ohio. The HyPER electrical hardware operates at power levels of approximately 100 kW, which is significantly less than the 2.6 MW STARC-ABL electrical system. As such, the HyPER test is set up as a "subscale" HIL test of the STARC-ABL power system. HyPER electrical hardware includes shaft-mounted electric machines, power converters, power supplies, power distribution cables, and an energy storage device, which can be

configured to represent a variety of EAP architectures (Ref. 25). It also includes an integrated real-time computer system that hosts EAP control software and turbomachinery simulations. This enables the electrical system and rotating shafts of EAP designs to be implemented in actual hardware and integrated with turbomachinery simulations and system-level control logic implemented in software. In this form, HyPER provides a HIL test configuration enabling the initial development and evaluation of EAP control technology in an environment that includes actual electrical system hardware.

6.1 Test Configuration

The HyPER STARC-ABL controls test configuration is shown in Figure 8. Here, a full-scale nonlinear simulation of the STARC-ABL turbomachinery and the control software are coded as a real-time application and implemented in a dSPACE SCALEXIO real-time computing system while a subscale version of the turbofan 1 LP shaft, the tailfan shaft, and their attached electrical power string are implemented in hardware. The hardware configuration includes two rotating shafts, each with an attached pair of 66 kW electric machines and inverters. The inverters are configured to accept torque command inputs and supply speed feedback measurements to the dSPACE SCALEXIO. Two 100 kW bi-directional power supplies provide power to the inverters over 350 V DC power buses. Each physical shaft enables the emulation of an electrified turbomachinery shaft with one of the attached electric machines emulating the shaft dynamics and torque load while the other electric machine acts as a motor or generator.

A slight limitation for this test is that HyPER only contains two rotating shafts. Ideally, a three-shaft configuration is preferred for emulating all three electrified shafts of the STARC-ABL (e.g., turbofan 1 LP shaft and generator, turbofan

2 LP shaft and generator, and tailfan shaft and motor). Such a three-shaft configuration was used for previous testing of the STARC-ABL baseline control design in another NASA Glenn facility (Refs. 19 and 26). Given the HyPER two-shaft limitation, an implementation decision was made to only emulate power string 1 in actual hardware, while power string 2 was implemented entirely in simulation. For power string 1 emulation, one of the two available shafts was used for emulating the LP shaft of turbofan 1 and its generator. The remaining shaft was used for emulating the portion of the tailfan motor energized by power string 1 and the loading placed upon it by the tailfan. Overall, the two-shaft implementation was a minor impact as the symmetry within the system still allowed all subsystem failures and reversionary control modes to be tested. During testing, subsystem failures were emulated through logic included in the real-time computer that allowed electric machine torque commands to be abruptly stepped to zero. In this manner, the failure of either power string could be emulated by simultaneously stepping both its generator and motor commanded torque values to zero. This action eliminated all LP shaft HPX from the associated turbofan as well as all electrical power transferred to the associated tailfan motor winding. Using this strategy to emulate the failure of a single power string enabled evaluation of failure scenarios that resulted in the attached turbofan operating in control Mode 1, the companion turbofan in control Mode 2, and the tailfan in its control Mode 1. Alternatively, the same strategy could be applied to simultaneously fail both power strings, which would emulate a tailfan failure with both turbofans operating in control Mode 1.

To allow the STARC-ABL reversionary control design to be tested in HyPER without modification, several differences between the full-scale STARC-ABL and subscale HyPER implementation are accounted for. These include differences in

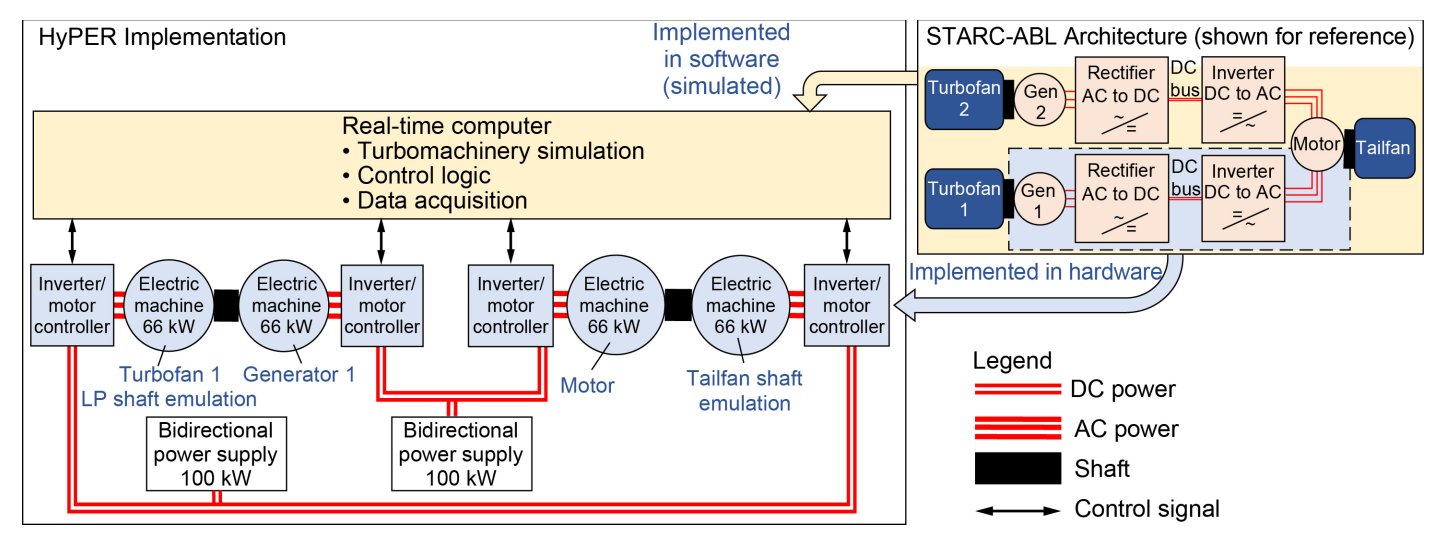


Figure 8.—HYPER STARC-ABL reversionary controls test configuration.

electric machine power levels, rated operating speeds, rotational shaft inertia, and viscous damping. To address these inconsistencies, an innovative adaptive sliding mode impedance controller with scaling (ASMICS) algorithm is applied (Ref. 27). This algorithm scales the torque and speed signals passed between the real-time computer and the electrical hardware. It also adjusts the torque commands supplied to the electric machines tasked with emulating turbomachinery shaft dynamics, which allows those machines to accurately represent specified subscale inertias and loads. With the inclusion of this technology, the evaluated reversionary control system perceived that it was controlling an actual full-scale STARC-ABL propulsion system.

The real-time application implemented on the dSPACE SCALEXIO provided integrated multifunctional capability (Ref. 26). This included real-time execution of the STARC-ABL nonlinear simulation, ASMICS, inverter communication, data acquisition, graphical user interface display drivers, plus the STARC-ABL reversionary control logic under test. All logic ran at a 15 ms control cycle update interval without issue.

6.2 Test Results

HyPER testing enabled comparison of the performance of the original baseline STARC-ABL control design presented in Reference 19 to the newly developed reversionary control design presented in this paper. It included a variety of nominal and failed operating scenarios conducted over multiple flight conditions. Figure 9(a) shows baseline control results from PLA burst/chop testing conducted at the SLS condition. Here, transient control performance is evaluated by introducing a PLA burst from idle to maximum throttle at time 40 s followed by a PLA chop from maximum throttle to idle at time 70 s. Figure 9(a) includes results from two separate tests—the first test performed with a power string 1 failure introduced at time 10 s and the second test with all subsystems performing nominally (failure-free). The top two rows of subplots show turbofan data with the thick blue and red lines reflecting the failure test case response of turbofan 1 and turbofan 2, respectively, while the thin yellow line reflects the nominal test case response of just turbofan 1. Turbofan 2 data are not shown for the nominal case as it closely matches that of turbofan 1 due to the symmetric nature of the STARC-ABL under nominal operating conditions. The bottom row of subplots shows tailfan data from the same two test cases with the thick blue lines reflecting the failure test case data and the thin yellow line reflecting nominal test case data. For the failure test case, a departure in the operation of the two turbofans is immediately apparent upon failure occurrence as turbofan 2 begins providing all power delivered to the tailfan. The system continues to operate post-failure up until the PLA chop is introduced. Then,

during the ensuing deceleration, a turbofan 1 LPC stall at time 73 s occurs and the HyPER test is halted.

Figure 9(b) shows results from the same test scenarios with the newly developed reversionary control logic enabled. In this case, the failure is promptly detected, and the subsystem controllers automatically switch to their appropriate reversionary control modes—turbofan 1 in Mode 1, turbofan 2 in Mode 2, and the tailfan in Mode 1. This applies revised turbofan VBV schedules, which allows the test to run to completion without encountering a turbofan 1 LPC stall. The reversionary control logic also applies an updated tailfan PLA-to- N_{tc} schedule that allows power string 2 to operate up to 125 percent power levels. This enables a 16 percent increase in the maximum tailfan net thrust output compared to the baseline control design.

Figure 10 shows analogous results for PLA burst/chop testing performed at a 37 k ft 0.78 Mach cruise condition, this time with a failure inserted in power string 2. Baseline control test results are shown in Figure 10(a). Here, it is observed that turbofan 1 experiences an HPC stall at approximately 44 s during the initial acceleration transient. This stall event is caused by an excessive generator HPX load placed upon the LP shaft of turbofan 1. If the resulting compressor stall leads to a turbofan 1 shutdown, all electrical power delivered to power string 1 will be lost. A loss of power string 1, coupled with the original power string 2 failure given in this example, will eliminate all electrical power delivered to the tailfan. This will result in a tailfan shutdown. If these cascading failures occur, the only remaining source of vehicle thrust will be turbofan 2 operating with no generator LP shaft HPX—a condition that places a turbofan at elevated risk for experiencing LPC stalls upon deceleration as was shown in Figure 9(a). The loss of turbofan 2 in this case would result in a catastrophic total vehicle loss of thrust.

Figure 10(b) shows results for this same 37 k ft 0.78 Mach cruise condition with the reversionary control enabled. In this case, the failure is properly detected, the subsystem controllers automatically enter their appropriate reversionary control modes to enable failure mitigation, and the acceleration and deceleration transients occur without issue. Here, a turbofan 1 HPC stall event during the acceleration is avoided due to the reversionary control's updated PLA-to- N_{tc} schedule that places a lower LP shaft HPX load on turbofan 1.

To further assess the robustness of the reversionary control logic, HyPER testing also included scenarios where failures were inserted during acceleration and deceleration transients. Figure 11 shows results for a power string 1 failure during an idle to maximum PLA acceleration transient at SLS conditions. Here, the transient starts at time 40 s and a failure occurs at time 42.1 s. The failure induces slight fluctuations in the system variables, but failure detection and reversionary control

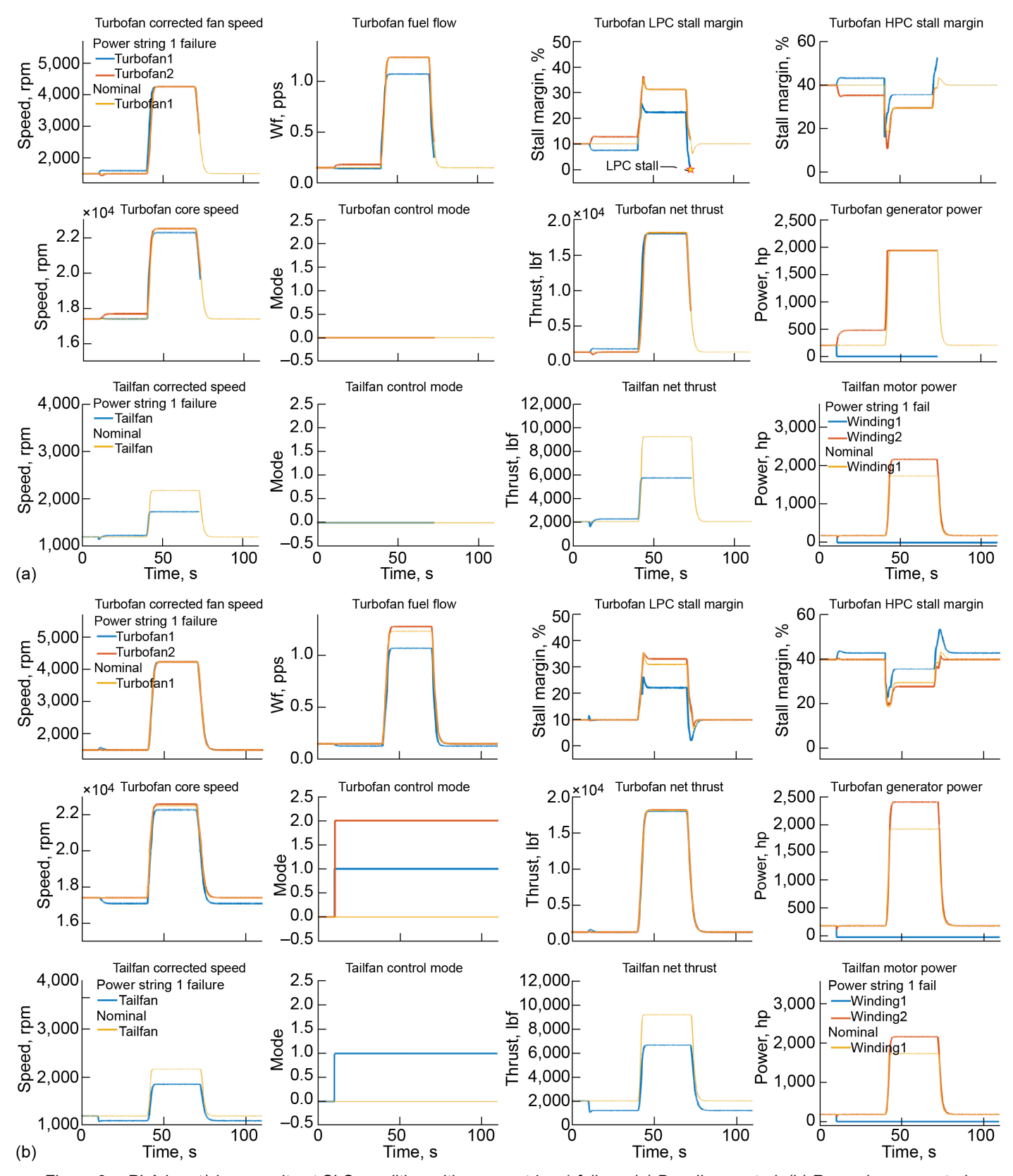


Figure 9.—PLA burst/chop results at SLS condition with power string 1 failure. (a) Baseline control. (b) Reversionary control.

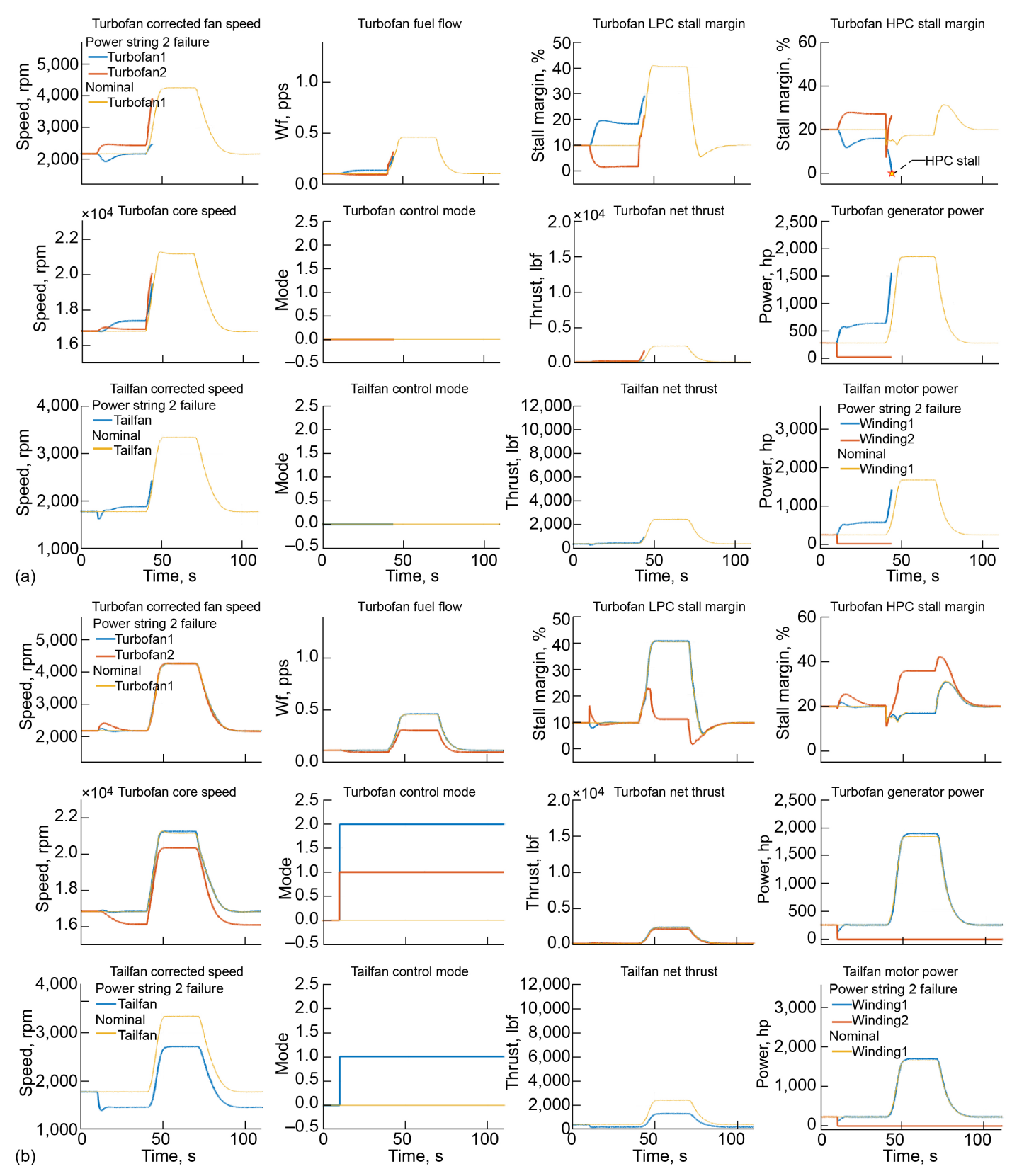


Figure 10.—PLA burst/chop results at cruise condition with power string 2 failure.(a) Baseline control. (b) Reversionary control.

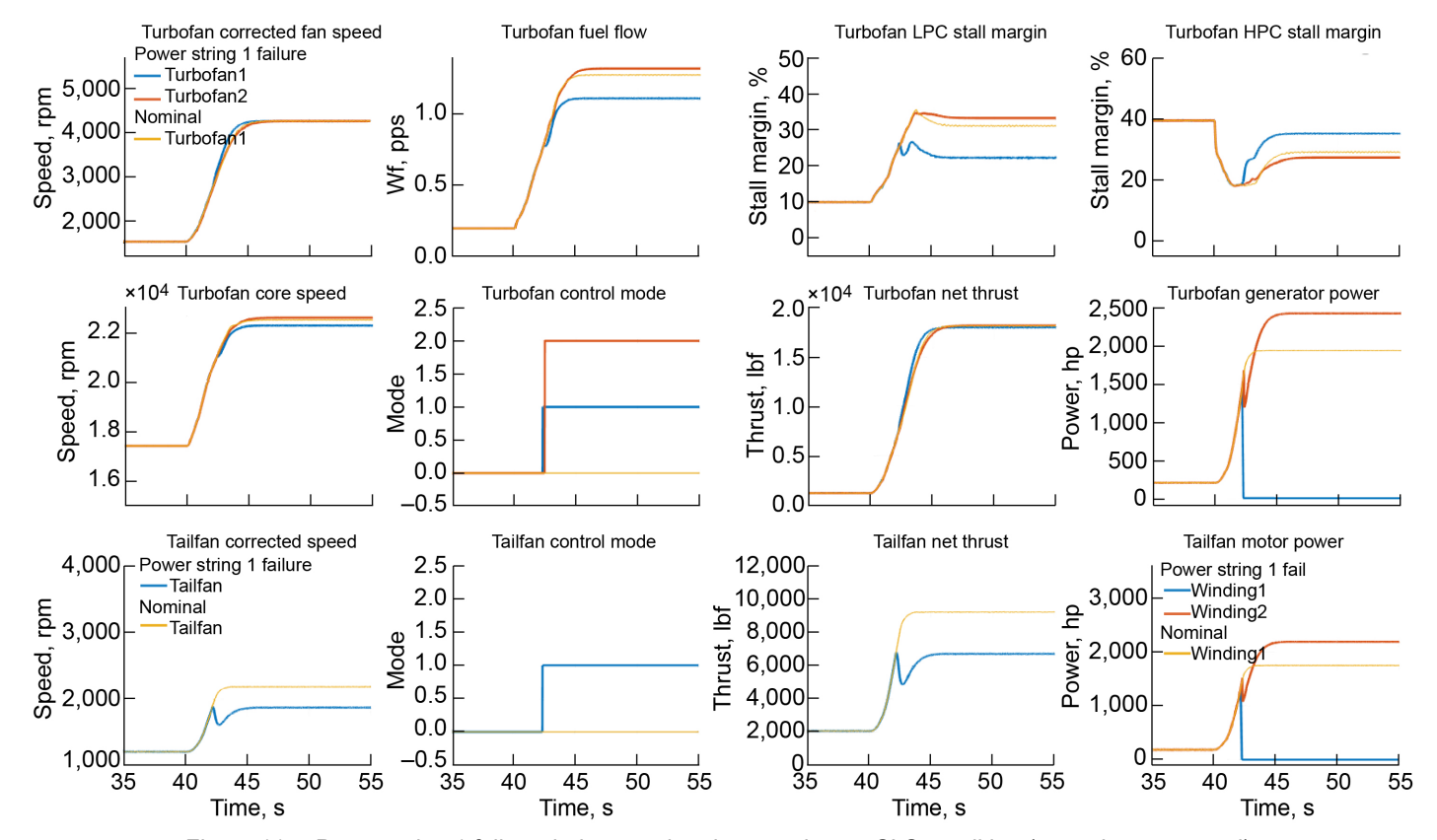


Figure 11.—Power string 1 failure during acceleration transient at SLS condition (reversionary control).

activation occur in adequate time to enable the transient to proceed without issue. Figure 12 shows analogous results for a power string 2 failure during a maximum to idle PLA deceleration transient performed at the 37 k ft 0.78 Mach condition. Once again, failure detection and reversionary control activation occur in ample time to enable the successful completion of the transient without issue.

The STARC-ABL's maximum net thrust output under both nominal and reversionary control operation was assessed throughout the vehicle's operating envelope. Results for the SLS and 37 k ft 0.78 Mach cruise conditions are shown in Table III and Table IV, respectively. Each table includes the percent of nominal maximum total vehicle thrust output of the vehicle and the subsystems when operating nominally and under failure conditions. At SLS the maximum total vehicle thrust output is 45,433 lbf. For the cruise condition, it is 7,171 lbf. In all failure cases the total vehicle net thrust remained above 50 percent of the nominal (failure free) operating condition. As expected, turbofan failures resulted in the largest thrust loss. In these cases, the total vehicle net thrust is 54.7 percent of nominal for the SLS condition and 51.1 percent of nominal for the cruise condition. For individual power system failures, the resulting total vehicle net thrust is 94.2 percent of nominal at SLS and 81.0 percent of nominal at cruise. For tailfan failure, the total vehicle net thrust was 79.0 percent of nominal at SLS and 59.7 percent of nominal at cruise.

TABLE III.—PERCENT MAXIMUM NET THRUST AT SLS

Thrust source	Failed subsystem, percent					
	No failure	Turbofan 1	Turbofan 2	Power Str. 1	Power Str. 2	Tailfan
Turbofan 1	39.8	0.0	39.9	39.5	39.9	39.5
Turbofan 2	39.8	39.9	0.0	39.9	39.5	39.5
Tailfan	20.3	14.8	14.8	14.8	14.8	0.0
Vehicle thrust	100.0	54.7	54.7	94.2	94.2	79.0

TABLE IV.—PERCENT MAXIMUM NET THRUST AT CRUISE

Thrust	Failed subsystem, percent					
source	No failure	Turbofan 1	Turbofan 2	Power Str. 1	Power Str. 2	Tailfan
Turbofan 1	33.0	0.0	33.1	29.8	33.1	29.8
Turbofan 2	33.0	33.1	0.0	33.1	29.8	29.8
Tailfan	34.0	18.0	18.0	18.0	18.0	0.0
Vehicle thrust	100.0	51.1	51.1	81.0	81.0	59.7

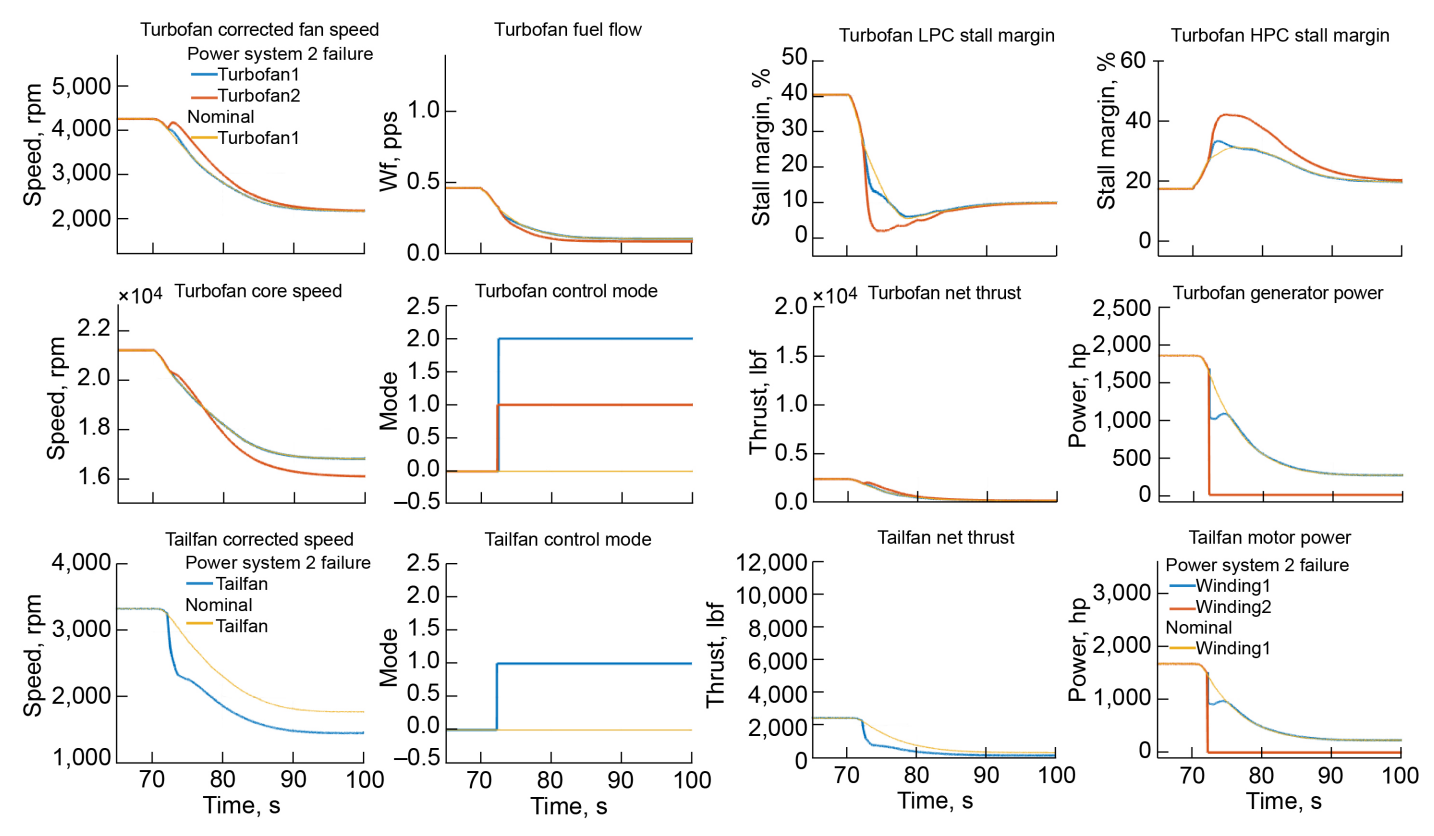


Figure 12.—Power string 2 failure during deceleration transient at cruise condition (reversionary control).

7.0 Discussion

The reversionary control study presented in this paper illustrates several of the challenges and potential solutions associated with failure mitigation in EAP architectures. However, the study is admittedly a high-level initial investigation of the overall problem, and much work remains. The subsystem failure types evaluated consisted of abrupt failures resulting in a complete loss of subsystem functionality. A practical failure mitigation approach would also require capabilities to mitigate more nuanced failure modes such as failures evolving more gradually or resulting in a partial loss of subsystem functionality. This might require blended control mode functionality and more sophisticated failure detection logic. Also, the study did not consider turbomachinery performance deterioration effects; it only turbomachinery of nominal (undeteriorated) health conditions. Further evaluation of the control design is needed to ensure that operability is maintained under all deterioration levels from nominal through end-of-life conditions. This study did consider an architectural change to the baseline STARC-ABL to facilitate failure mitigation that resulted in the power system being partitioned into two parallel strings. However, a more thorough systems engineering approach could likely identify

additional architectural changes to provide added robustness and failure mitigation functionality.

8.0 Conclusions

A reversionary control strategy for maintaining operability of an electrified aircraft propulsion (EAP) concept in the presence of subsystem failures was presented. The approach was applied to a distributed partially turboelectric propulsion architecture consisting of two turbofan engines that produce thrust and supply mechanical offtake power for the generation of electricity supplied to a motor-driven tailfan propulsor. This effort demonstrated the operability concerns posed by subsystem failures in an EAP architecture that exhibits tight integration and coupling between subsystems. If unmitigated, such failures can cause engine compressor stalls, engine shutdowns, and cascading failures sometimes with catastrophic consequences. Presented failure detection logic and reversionary control modes included in the propulsion control system were shown to successfully mitigate the effects of such failures, allowing the system to continue to operate and produce thrust. A real-time hardware-in-the-loop test of the integrated control design demonstrated robust transient system operation in the presence of realistic electrical system variations.

References

- Jansen, R.H., Bowman, C., Jankovsky, A., Dyson, R., Felder, J., (2017), "Overview of NASA Electrified Aircraft Propulsion Research for Large Subsonic Transports," AIAA-2017-4701, AIAA Propulsion and Energy Forum, Atlanta, GA, July 10–12.
- National Academies of Sciences, Engineering, and Medicine. 2016. Commercial Aircraft Propulsion and Energy Systems Research: Reducing Global Carbon Emissions. Washington, DC: The National Academies Press. https://doi.org/10.17226/23490.
- SAE International Aerospace Recommended Practice, (2010), "Guidelines for Development of Civil Aircraft and Systems," SAE Standard ARP4754A, December 2010.
- SAE International Aerospace Recommended Practice, (1996), "Guidelines and Methods for Conducting the Safety Assessment Process on Civil Airborne Systems and Equipment," SAE Standard ARP4761, December 1996.
- Courtin, C., Hansman, R.J., (2018), "Safety Considerations in Emerging Electric Aircraft Architectures," AIAA-2018-4149, Aviation Technology, Integration, and Operations Conference, Atlanta, GA, Jun. 25–29.
- Simon, D.L., and Connolly, J.W., (2020), "Electrified Aircraft Propulsion Systems: Gas Turbine Control Considerations for the Mitigation of Potential Failure Modes and Hazards," ASME-GT2020-16335, ASME Turbo Expo Conference, Virtual, Online, September 21–25.
- Zhang, D., Xu, Y., Zhang, Z., Dong, D., Cao, Y., Mcginnis, P., Keck, B. (2023), "A Solid-State Circuit Breaker for Hybrid Electric Propulsion," AIAA 2023-4155, AIAA Aviation Forum, San Diego, CA, Jun. 12–16.
- Flynn, M.C., Jones, C., Rakhra, P., Norman, P., and Galloway, S. (2017), "Impact of Key Design Constraints on Fault Management Strategies for Distributed Electrical Propulsion Aircraft," AIAA-2017-5034, 53rd AIAA/SAE/ ASEE Joint Propulsion Conference, Atlanta, GA, Jul. 10–12.
- Kuhlberg, J.F., Newirth, D.M., Kniat, J., and Zimmerman, W.H. (1984), "Integration of the PW2037 Engine Electronic Control System in the Boeing 757 Airplane," SAE Technical Paper No. 841554, Aerospace Congress & Exposition, Long Beach, CA, Oct. 15–18.
- Bosco, C.J., "Certification Issues For Electrical and/or Electronic Engine Controls," SAE Paper 871844, Aerospace Technology. Conference and Exposition, Long Beach, CA, Oct. 5–8, 1987.
- Evans, J.F.O., "Fault Trees and System Reliability Analysis with Reference to the Control of Aircraft Engines," AGARD-LS-113, Microcomputer Applications in Power and Propulsion Systems, March 1981.

- 12. Kratz, J.L., and Simon, D.L., (2024), "Failure Behavior and Control-Based Mitigation for a Parallel Hybrid Propulsion System," AIAA-2014-0522, AIAA SciTech Forum, Orlando, FL, Jan. 8–12.
- Kratz, J.L., and Simon, D.L., (2022), "Failure Modes and Mitigation Strategies for a Turboelectric Aircraft Concept with Turbine Electrified Energy Management," AIAA-2022-1191, AIAA SciTech Forum, San Diego, CA, Jan. 3–7.
- Welstead, J.R., Felder, J.L., (2016), "Conceptual Design of a Single-Aisle Turboelectric Commercial Transport with Fuselage Boundary Layer Ingestion," AIAA 2016-1027, AIAA SciTech Forum, 54th AIAA Aerospace Sciences Meeting, San Diego, CA, January 4–8.
- 15. Felder, J.L., Schnulo, S.L., Tong, M.T., Berton, J.J., Thacker, R.P., Haller, W.J. (2022), "An Updated Assessment of Turboelectric Boundary Layer Ingestion Propulsion Applied to a Single-Aisle Commercial Transport," AIAA SciTech Forum and Exposition, San Diego, CA, January 3–7.
- Kratz, J.L., Culley, D.E., and Thomas, G.L., (2019), "A Control Strategy for Turbine Electrified Energy Management," AIAA–2019–4499 AIAA/IEEE Electric Aircraft Technologies Symposium (EATS), Indianapolis, Indiana, August 22–24.
- 17. Litt, J.S., Sachs-Wetstone, J.J., Simon, D.L., Sowers, T.S., Owen, A.K., Bell, M.E., Guthrie, B.E., Lehan, J. and Castro, A., (2023), "Flight Simulator Demonstration and Certification Implications of Powertrain Failure Mitigation in a Partial Turboelectric Aircraft," AIAA 2023-4156, AIAA/IEEE Electrified Aircraft Technology Symposium (EATS), San Diego, CA, Jun. 12–16.
- Lytle, J., Follen, G., Naiman, C., Evans, A., Veres, J., Owen, K., Lopez, I., (2000), "Numerical Propulsion System Simulation (NPSS) 1999 Industry Review," NASA/TM-2000-209795, August.
- Simon, D.L., Bianco, S.J., Horning, M.A., (2023), "Integrated Control Design for a Partially Turboelectric Aircraft Propulsion System," ASME-GT2023-100921, ASME Turbo Expo Conference, Boston, MA, June 26–30.
- Chapman, J.W., Lavelle, T.M., May, R.D., Litt, J.S., Guo, T-H., (2014), "Toolbox for the Modeling and Analysis of Thermodynamic Systems (T-MATS) User's Guide," NASA/TM-2014-216638, January.
- Chapman, J.W., Litt, J.S., (2018), "An Approach for Utilizing Power Flow Modeling for Simulations of Hybrid Electric Propulsion Systems," AIAA-2018-5018, AIAA Propulsion and Energy Forum, Cincinnati, OH, July 9–11.
- 22. Jaw, L., and Mattingly, J., (2009), "Aircraft Engine Controls," New York, NY, USA: American Institute of Aeronautics and Astronautics.

- May, R.D., Garg, S., (2012), "Reducing Conservatism in Aircraft Engine Response Using Conditionally Active Min-Max Limit Regulators," ASME GT2012-70017, ASME Turbo Expo, Copenhagen, Denmark, June 11–15.
- 24. Scoles, R.J., 1986, "FADEC Every Jet Engine Should Have One," SAE Paper 861802.
- Buescher, H.E., Culley, D.E., Bianco, S.J., Connolly, J.W., Dimston, A.E., Saus, J.R., Theman, C.J., Horning, M.A., and Purpera, N.C., (2023), "Hybrid-Electric Aero-Propulsion Controls Testbed: Overview and Capability," AIAA 2023-0671, AIAA SciTech Forum, January 23–27.
- 26. Simon, D.L., Bianco, S.J., Horning, M.A., Saus, J.R., Amthor, A.E., Sachs-Wetstone, J.J., (2023), "Real-time Hardware-in-the-Loop Evaluation of a Partially Turboelectric Propulsion Control Design," AIAA 2023-4235, AIAA/IEEE Electric Aircraft Technologies Symposium (EATS), San Diego, California, June 12–16.
- 27. Bianco, S.J., Simon, D.L., Hill, E.D, (2024), "Adaptive Control and Scaling Approach for the Emulation of Dynamic Subscale Torque Loads," AIAA-2024-2356, AIAA SciTech Forum, Orlando, FL, Jan. 8–12.